

Dynamic characterization of growth and gene expression using high-throughput automated flow cytometry

Ignacio A Zuleta^{1,2}, Andrés Aranda-Díaz^{1,2}, Hao Li^{1,2} & Hana El-Samad^{1,2}

Cells adjust to changes in environmental conditions using complex regulatory programs. These cellular programs are the result of an intricate interplay between gene expression, cellular growth and protein degradation. Technologies that enable simultaneous and time-resolved measurements of these variables are necessary to dissect cellular homeostatic strategies. Here we report the development of an automated flow cytometry robotic setup that enables real-time measurement of precise and simultaneous relative growth and protein synthesis rates of multiplexed microbial populations across many conditions. These measurements generate quantitative profiles of dynamically evolving protein synthesis and degradation rates. We demonstrate this setup in the context of gene regulation of the unfolded protein response (UPR) of *Saccharomyces cerevisiae* and uncover a dynamic and complex landscape of gene expression, growth dynamics and proteolysis following perturbations.

In response to perturbations in their environment, cells undergo physiological changes that involve intricate modulations of their growth programs and the composition of their proteome. It has long been appreciated that both types of change are necessary to restore cellular homeostasis¹. Nonetheless, altered growth in response to perturbations, on the one hand, and protein synthesis and degradation rates, on the other, are themselves dynamically interlinked.

Although many quantitative approaches to measure gene expression exist, they are limited by their bulk nature, throughput or time resolution. Quantification of complex gene expression and growth phenotypes in microbial cultures can be achieved using a combination of time-lapse fluorescence microscopy², flow cytometry³, DNA microarrays⁴, RNA-seq⁵ and DNA barcode arrays⁶. Microarray-based approaches and whole-transcriptome sequencing have excellent gene throughput and dynamical range but are inherently a bulk measurement and typically lack fine time resolution. By contrast, time-lapse fluorescence measurement of cell populations inside microfluidics devices⁷ yields single-cell information but is usually low throughput and subject to micro-environment inhomogeneity and light-induced stress⁸. In micro-organisms, e.g., *Saccharomyces cerevisiae*, flow cytometry allows

easy measurement of phenotypic variables such as protein abundance and cell-to-cell variability across a population for about half the genome⁹. Nevertheless, widespread study of dynamics using flow cytometry is limited by the lack of hardware tools that allow for reproducible measurement of cell cultures in microwell plates with low well-to-well variability and fine time resolution.

Here we introduce an automated flow cytometry system that achieves such measurements, and we demonstrate its capabilities by determining quantitative instantaneous growth rates, protein synthesis rates and differential fluorescent-protein degradation fluxes. In addition, this setup achieves facile quantification of time-resolved multidimensional dose responses for many phenotypes, enabling in-depth studies of cellular connectivity and dynamic regulation.

RESULTS

High-throughput monitoring of microbial culture dynamics

Simultaneous high-throughput measurement of growth and gene expression is challenging. For example, simple bulk growth and fluorescence measurements using plate readers suffer from poor reproducibility^{10,11}. Although substantial progress has been made in time resolution using microfluidics¹² and chemostats^{13,14}, these technologies are limited in their ability to achieve simultaneous growth and gene expression measurements in high throughput at the single-cell level (**Fig. 1a**). With the technology described here, we can achieve measurements with a resolution of 10 s per sample or about 20 min per 96-well plate. To enable such measurements, we developed a measurement setup that integrates a flow cytometer, a liquid handler and a deep-well-plate incubator using a robotic arm and custom control software (**Fig. 1b** and Online Methods). Briefly, culture samples are continuously transferred to a shallow 96-well plate, which is then moved by the robot to the flow cytometer for measurement (**Fig. 1c**). This sequence of events is repeated to carry out facile and reproducible stimulus-response experiments to explore phenotypes across time and stimulus dose (**Fig. 1d**). A typical experiment consists of two stages: an outgrowth phase wherein cells are brought to exponential growth, which is followed by a stimulus event wherein a treatment solution is added after the appropriate growth state has been achieved. After the stimulus event, we continuously monitor the

¹Department of Biochemistry and Biophysics, University of California, San Francisco, San Francisco, California, USA. ²The California Institute for Quantitative Biosciences, San Francisco, California, USA. Correspondence should be addressed to H.E.-S. (hana.el-samad@ucsf.edu) or H.L. (haoli@genome.ucsf.edu).

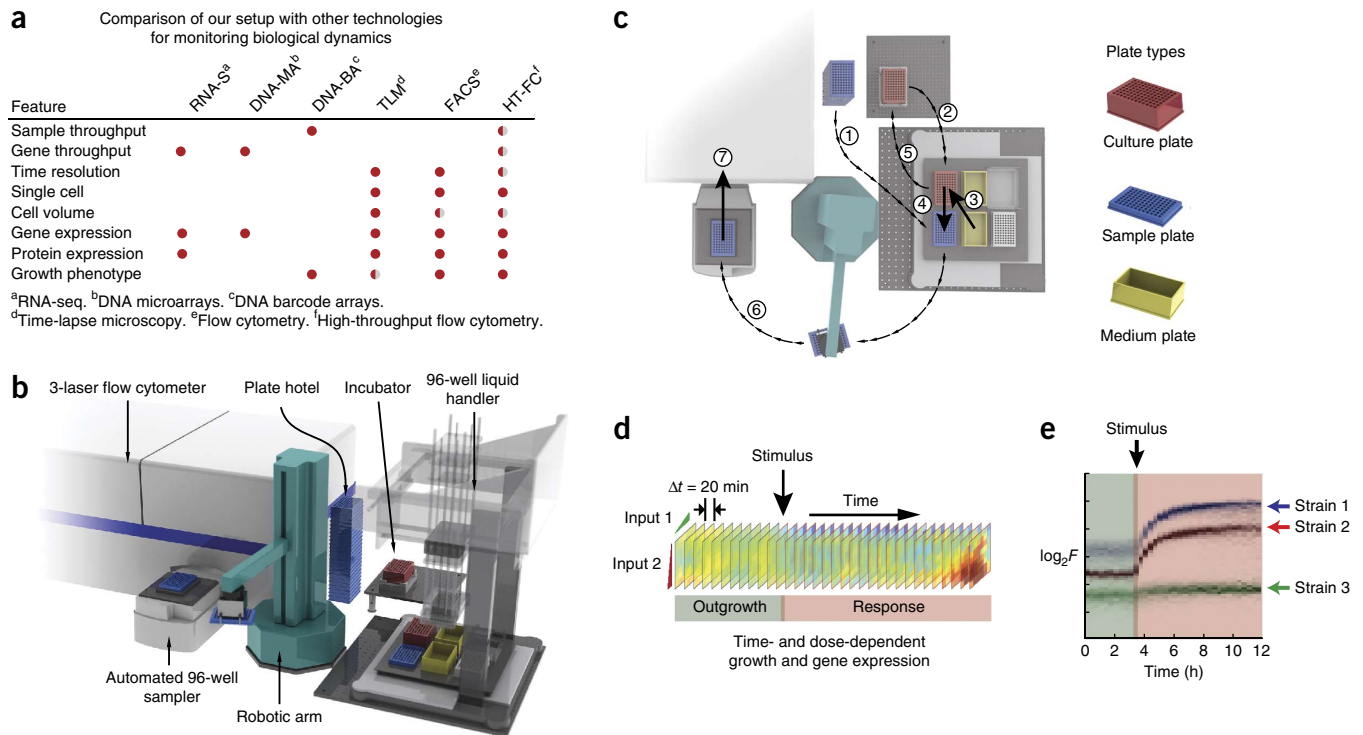


Figure 1 | Automated high-throughput real-time flow cytometry. **(a)** Comparison of high-throughput flow cytometry (HT-FC) robotic setup with other technologies (full circle, good; semicircle, fair; no circle, poor). **(b)** Hardware arrangement for HT-FC system. **(c)** Sequence of main events in a typical experiment. Steps 1–7 repeat every 20 min and involve (1) loading a fresh sample plate into the liquid handler, (2) removal of the culture from the incubator, (3) addition of fresh medium and stimulus to the culture, (4) taking of a sample from the culture, (5) returning the culture to the incubator, (6) transport of the sample plate to the high-throughput sampler and (7) measurement of the sample plate in the flow cytometer. **(d)** Time- and dose-dependent dynamical portraits can be acquired with HT-FC. **(e)** An example in which the fluorescence of three strains is monitored over time after a perturbation.

culture evolution during the response period (**Fig. 1e**). Treatment and/or culture conditions are automatically maintained through the experiment (up to 24 h) by adding the stimulus at its nominal concentration to compensate for dilution (**Supplementary Fig. 1a**). Different stimuli such as pulses, nutrient depletions and ramps can also be easily implemented with high sample-to-sample and day-to-day reproducibility and no well-to-well carry-over (**Supplementary Fig. 1b–d**). Additionally, several strains can be simultaneously cultured (multiplexed) in one well for internally controlled measurements of differential phenotypes under many conditions.

Quantification of protein expression rates

A confounding factor in interpreting protein synthesis rates using fluorescent reporters is the interdependence between the measured fluorescence and growth dynamics when perturbations affect growth. Here we define growth slowdown as the decrease in the rate of cell division as measured by the time-dependent accrual of the number of cells. Because the concentration of any cellular moiety can be affected by both its turnover dynamics^{15,16} and the dynamics of cell growth, slowdown after stress may cause fluorescent proteins to accumulate^{17–19}, resulting in inflated estimates of gene expression or protein synthesis rate.

We studied the instantaneous growth phenotype associated with increasing doses of tunicamycin-induced endoplasmic reticulum (ER) stress in the yeast *S. cerevisiae*. When cells are exposed to tunicamycin, they turn on the expression of about 200 genes in what is known as the UPR^{20–23}. Concomitantly, cells slow down

growth and reduce the translational flux of proteins targeted to the secretory pathway, presumably as a way to avoid the accumulation of misfolded proteins^{24,25}. To quantify the cell's response to this ER stress, we used a transcriptional reporter consisting of a synthetic promoter that contains four copies of the UPR-1 (UPR element 1) motif fused to a GFP-coding sequence²⁶.

The rate of change of fluorescence in the culture is the result of production and disappearance of the fluorophore:

$$\frac{dF_{\text{GFP,total}}}{dt} = \alpha_{4\text{XUPRE,total}}(t) - \beta_{\text{GFP,total}}(F, t) \quad (1)$$

$F_{\text{GFP,total}}$ is the total instantaneous fluorescence in the culture, $\alpha_{4\text{XUPRE,total}}(t)$ is the protein synthesis rate associated with the UPR reporter and $\beta_{\text{GFP,total}}(F, t)$ is the degradation flux of the fluorescent protein. Because $F_{\text{GFP,total}} = N(t) \times \langle F_{\text{GFP,cell}} \rangle$, where $N(t)$ is the number of cells in the culture and $\langle F_{\text{GFP,cell}} \rangle$ is the instantaneous average fluorescence per cell in the population, we write a general expression for the average protein synthesis rate per cell in terms of the measured fluorescence and cell number (see **Supplementary Note**):

$$\frac{d\langle F_{\text{GFP,cell}} \rangle}{dt} = \alpha_{4\text{XUPRE,cell}}(t) - \beta_{\text{GFP,cell}}(F, t) - \gamma(t) \times \langle F_{\text{GFP,cell}} \rangle \quad (2)$$

In this equation, the impact of growth rate on the change of GFP signal per cell is captured by the cell division rate $\gamma(t)$, defined

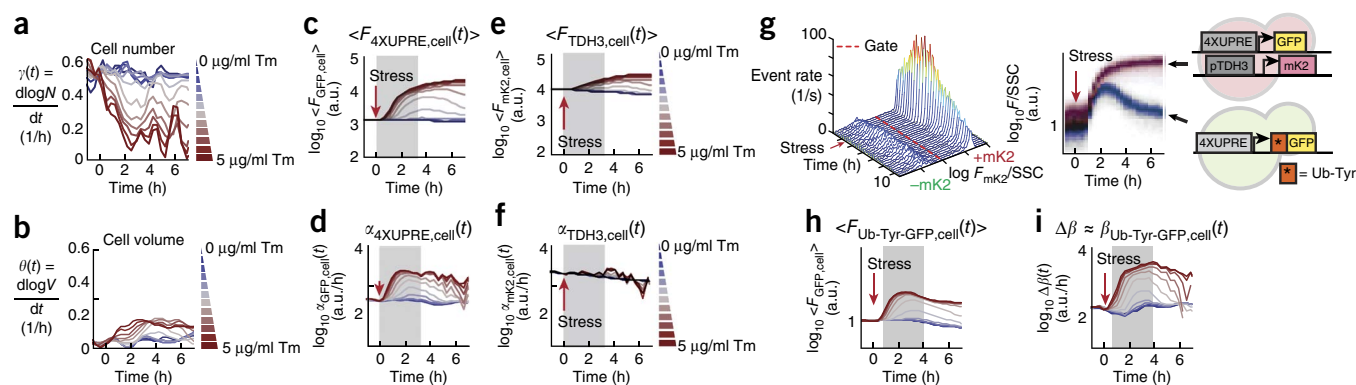


Figure 2 | Growth rate-corrected reporter protein dynamics by high-throughput flow cytometry. (**a,b**) Rate of change for cell number N (γ ; **a**) and for average volume V (θ ; **b**) for yeast cells stressed with tunicamycin (Tm). (**c,d**) Average fluorescence measurement (F ; **c**) and growth-corrected expression rate of the p4XUPRE-GFP transcriptional reporter (α_{4XUPRE} ; **d**) in yeast cells. Shaded areas indicate integration windows for two-dimensional dose-response plots. (**e,f**) Average fluorescence (**e**) and growth-corrected expression rate of pTDH3-mKate2 (α_{TDH3} ; **f**): $TDH3$ is a housekeeping gene. (**g**) Left, distributions of red fluorescence across time for a mixture of two strains in a competition experiment; the strains are distinguished by the presence of a pTDH3-mKate2 (mK2) fluorescent tag. Right, green fluorescence signal in the two strains, containing GFP (red population) or a short-lived allele Ub-Tyr-GFP (blue population), both driven by the UPR synthetic promoter 4XUPRE (far right). SSC, side scatter. (**h**) Raw average fluorescence for the unstable GFP allele for different doses of Tm (scale as in **a**). (**i**) Differential degradation flux of the unstable allele Ub-Tyr-GFP as a function of time. The experiment was replicated twice. a.u., arbitrary units.

as the time derivative of the logarithm of the measured number of cells, $d\log N/dt$ (Fig. 2a). A similar equation can be derived for the change of GFP concentration (GFP per unit volume), in which the change of cell volume also contributes to the dilution (Online Methods). This contribution can be quantified by the cell volume accumulation rate $\theta(t)$, defined as $d\log\langle V \rangle/dt$ (where $\langle V \rangle$ is the average cell volume), which can be a substantial contribution to biomass accrual rate when cells abruptly stop dividing (Fig. 2b). The average cell volume can be estimated using the cell's light scattering (Online Methods and Supplementary Fig. 2). However, the relationship between volume^{27–29} or cell cycle³⁰ and scatter parameters can be complex and should be calibrated for each cell type and experimental condition.

Equation (2) indicates that the instantaneous rate of change of fluorescence (Fig. 2c), $d\langle F_{GFP,cell} \rangle/dt$, is equal to the balance of the instantaneous protein synthesis rate $\alpha_{4XUPRE,cell}(t)$ (Fig. 2d); its decrease due to cell division, $-\gamma(t) \times \langle F_{GFP,cell} \rangle$; and its disappearance by degradation, $\beta_{GFP,cell}(F, t)$. If the fluorescent reporter is stable, its 'degradation flux' $\beta_{GFP,cell}(F, t)$ is negligible. In this case, the instantaneous protein synthesis rate can be extracted from the fluorescence measurements and cell division rate, both measured in the same experiment. The estimated instantaneous protein synthesis rate, $\alpha_{4XUPRE,cell}(t)$, is a time-dependent, population-averaged effective rate of production of the fluorescent protein that can be interpreted as a lumped rate of transcription, translation and folding.

Our data indicate that after perturbation by tunicamycin, the UPR reporter undergoes a transient pulse of expression whose magnitude and duration depends on the extent of the stress (Fig. 2d). In particular, for low ($<0.04 \mu\text{g/ml}$) and medium ($0.04\text{--}0.08 \mu\text{g/ml}$) doses of tunicamycin, these measurements traced the attenuation of UPR activation following homeostatic recovery. For high doses ($0.15\text{--}5 \mu\text{g/ml}$), some UPR attenuation still occurred. A colony-counting assay revealed that cell death did not occur at these doses (Supplementary Fig. 3a,b), which suggests that this UPR attenuation is likely the consequence of global

gene expression and growth arrest. The results of the colony-counting assay also quantitatively validate the growth measurements obtained with our setup (Supplementary Fig. 3c).

Raw fluorescence measurements of a transcriptional reporter for $TDH3$, a housekeeping gene³¹, showed a stress-induced dose-dependent increase (Fig. 2e). By contrast, the growth-corrected instantaneous protein synthesis rate of pTDH3-mKate2 showed no change at early times for any dose (Fig. 2f), and data became noisy at later time points for the high-stress condition because of low cell counts (see also Supplementary Fig. 4). Notably, this instantaneous protein synthesis rate measurement does not depend on any normalization, in contrast to previous measures of gene expression that need to be normalized by the total RNA abundance or a control that is assumed to be constitutively expressed. Taken together, these data highlight the fact that complex growth dynamics during perturbation experiments need to be integrated into analyses for the quantitative determination of gene expression profiles.

Quantification of relative protein degradation rates

Control of protein degradation is a crucial layer of regulation determining effective gene dosage for many genes^{32–35}. Our analysis can be easily extended to calculate relative degradation flux for unstable proteins.

We cocultured two yeast strains containing the synthetic UPR promoter. In the first strain, the promoter is driving a long-lived GFP. In the second strain, the same promoter is driving an unstable GFP allele, ubiquitin (Ub)-Tyr-GFP³⁶, containing a destabilizing tyrosine residue³⁷ that is unmasked by Ubp1 (refs. 38,39). We distinguished the two strains using an mKate2 (ref. 40) fluorescently label: the stable GFP strain expresses mKate2 constitutively from a $TDH3$ promoter, whereas the strain containing the Ub-Tyr-GFP allele lacks mKate2 expression (Fig. 2g). The basal fluorescence intensity of the unstable allele was lower than that of the stable allele, and after induction by tunicamycin, it decreased after peaking. As both strains have the same genetic background,

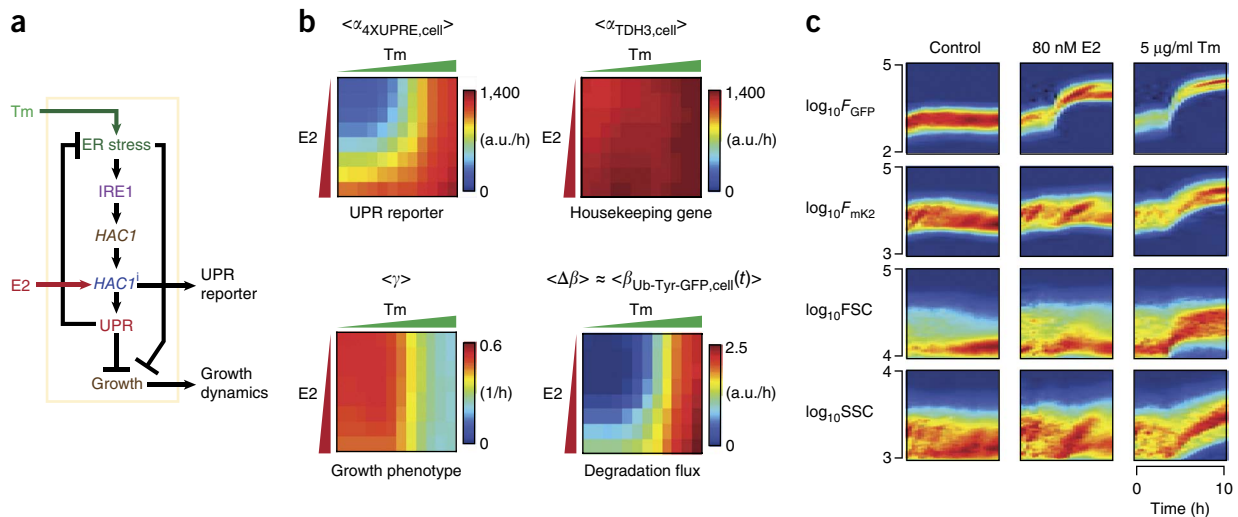


Figure 3 | Determination of two-dimensional dose responses and cell-to-cell variability by high-throughput flow cytometry. **(a)** Strategy for perturbation of the UPR pathway using an environment input (tunicamycin, Tm) and a synthetic input (an inducible spliced allele of *HAC1*). Transmembrane nuclease IRE1 senses luminal-side ER stress and splices *HAC1* mRNA when activated. **(b)** Heat maps show the protein synthesis rate of the 4XUPRE reporter (α_{4XUPRE}) and pTDH3 (α_{TDH3}), the growth phenotype (γ) and the differential degradation flux ($\Delta\beta$) for every dose of Tm and estradiol (E2). The data are reported as an average over a time window of 3 h. **(c)** Time-dependent distributions of single-cell green fluorescence (F_{GFP}), red fluorescence (F_{mk2}), forward scatter (FSC) and side scatter (SSC) for no treatment (left), 80 nM E2 (center) and 5 $\mu\text{g/ml}$ Tm (right).

are in the same culture and have reporters under control of the same promoter (**Supplementary Table 1** and **Supplementary Fig. 5a**), we assume that the decrease in fluorescence is reflective of the faster degradation of the unstable allele (**Fig. 2h**). In this scenario, we can use a differential form of the protein turnover model (equation (1)) to compute a relative dose-dependent degradation flux $\Delta\beta$ per cell for the unstable allele (**Fig. 2i** and **Supplementary Note**):

$$\Delta\beta(t) = -\Delta\left(\frac{d\langle F \rangle}{dt}\right) - \gamma(t) \times \Delta\langle F \rangle \quad (3)$$

where $\Delta\beta(t) = \beta_{\text{Ub-Tyr-GFP,cell}}(F, t) - \beta_{\text{GFP,cell}}(F, t)$; $\Delta(d\langle F \rangle/dt) = d\langle F_{\text{Ub-Tyr-GFP,cell}} \rangle/dt - d\langle F_{\text{GFP,cell}} \rangle/dt$; and $\Delta\langle F \rangle = \langle F_{\text{Ub-Tyr-GFP,cell}} \rangle - \langle F_{\text{GFP,cell}} \rangle$. For a stable reference protein, this expression implies that $\beta_{\text{Ub-Tyr-GFP,cell}} \approx -\gamma \times \Delta\langle F \rangle$ at steady state. According to the expression in equation (3), the calculated degradation flux increases under ER stress in a dose- and time-dependent fashion (**Fig. 2i**), as has been previously observed during ER stress^{22,41–44}. Our measurements provide a quantitative and dynamic window into the regulation of ER-associated degradation^{42,45} and its relationship with cytosolic protein degradation. Furthermore, because degradation flux is a function of substrate concentration $\langle F_{\text{Ub-Tyr-GFP,cell}} \rangle$, these measurements enabled us to establish the regime in which the degradation of a given substrate has first-order kinetics (**Supplementary Fig. 5b**). This general approach, as opposed to methods based on bleaching and recovery^{46,47}, enables the quantification of protein degradation *in vivo*, quantitatively and in real time. Unlike traditional pulse-chase approaches⁴⁶, our approach is not destructive⁴⁸, and, because it does not have the dead-time limitation of bleaching-based microscopy approaches⁴⁷, it allows for transient measurements of degradation flux.

Automated measurement of multidimensional dose responses

Measurement of dose responses is a powerful tool to establish the input-output mapping of biological modules, such as for

gene promoters^{49,50} or stress pathways¹, and for the efficient constraining of complex dynamical models^{51,52}. Furthermore, combinatorial stimulation is an emerging powerful approach for interrogating the logic of cellular pathways⁵³. As a first proof of concept, we measured the dose-response dependency of the UPR reporter protein synthesis rate for many combinations of tunicamycin-induced ER stress and synthetic transcriptional activation (**Fig. 3a**). We achieved synthetic activation using an estradiol-inducible system^{54–56} wherein the addition of estradiol at different doses induces the expression of an active allele of *HAC1*, *HAC1*ⁱ, which encodes the main transcription factor controlling the UPR. In this experiment, we again multiplexed two strains, both of which contain an estradiol-inducible system driving expression of the *HAC1*ⁱ allele. In addition, one of the strains contains a stable allele of GFP driven by a synthetic UPR reporter, whereas the second strain contains a destabilized allele of GFP and is further labeled by pTDH3-mKate2. We measured time-dependent growth, reporter protein synthesis rate and degradation flux for 96 combinations of the two inputs, estradiol and tunicamycin, for the two strains multiplexed in the same well. For easy visualization, we summarized these quantities by time-averaging for 3 h after induction (see **Fig. 2**) in order to establish the two-dimensional dose responses of four different phenotypic variables: α_{TDH3} , α_{4XUPRE} , γ and $\Delta\beta$ (**Fig. 3b**).

As expected, the rate of protein synthesis from the UPR reporter (α_{4XUPRE}) increased with both expression of *HAC1*ⁱ and tunicamycin-induced ER stress (**Fig. 3b**). Nonetheless, synthetic activation with the inducible system generated a slightly lower UPR reporter protein synthesis rate than did stress-induced activation. Simultaneous full activation with both ER stress and *HAC1*ⁱ expression yielded a similar protein synthesis rate to that of activation with ER stress alone. This is consistent with a model in which both ER stress and the dose of *HAC1*ⁱ expression modulate the UPR independently and generate different growth phenotypes. Here again, the growth-corrected TDH3 rate of protein synthesis was constant

after stress or UPR overactivation (Fig. 3b). This, together with the observation that cells were viable after removal of stress in our plating assay (Supplementary Fig. 3b), revealed that the cell's protein synthesis capacity was not saturated in these regimes and suggests that the observed growth phenotype resulted from arrest in the cell cycle and not a failure to accumulate biomass.

Moreover, whereas ER stress caused a major growth defect (Fig. 3b), *HAC1*¹ overexpression caused only a transient pause in cell division rate $\gamma(t)$ that was offset by cell volume growth $\theta(t)$ (Supplementary Fig. 6). Degradation flux was also dependent on both tunicamycin and estradiol dosage, these results being consistent with a role for the UPR in modulating the degradation flux across all levels of stress (Fig. 3b).

Quantification of cell-to-cell variability

The regulatory response of a population of cells to environmental changes is often accompanied by a change in population structure that reflects changes in cell cycle and cellular growth. A unique strength of our flow cytometry setup is that it allows for quantifying both cell-to-cell variability in a population and changes in population structure as a function of time. For example, examination of p4XUPRE and pTDH3 fluorescence as a function of tunicamycin and estradiol doses showed the temporal emergence and disappearance of multimodal distributions (Fig. 3c and Supplementary Figs. 7 and 8). At the same time, forward-scatter (FSC) and side-scatter (SSC) signals revealed complex dynamics resembling the reporter protein synthesis rate of the constitutive gene (Supplementary Figs. 7c,d and 8c,d). Correction by SSC, for example, removed the multimodality and pointed to its root in the interplay of stress and growth (Supplementary Figs. 7e,f and 8e,f). Furthermore, our measurements indicated that although different inputs can result in the same steady-state mean fluorescence of p4XUPRE, the variability around this mean may vary depending on the nature of the stimulus (estradiol or tunicamycin, Fig. 3c and Supplementary Fig. 9). Quantification of cell-to-cell variability by the coefficient of variation (CV) as a function of mean for different doses of tunicamycin and estradiol (Supplementary Fig. 10) revealed that, even for the same input, fluorescence trajectories can have the same mean value at different time points but that the population distributions of these transient states can be different (Supplementary Fig. 11).

More quantitatively, we observed that, on average, the CV² of the UPR reporter fluorescence decreased as an inverse function of its mean at low levels of expression and reached a noise floor at high expression levels as expected from dominance of extrinsic cellular noise at these values (Supplementary Fig. 12). Dissection of this phenomenon, however, uncovered a fine microstructure in which the variability has different dependence on physical population parameters, such as SSC and FSC (Supplementary Fig. 13), according to the mode of stimulation. Specifically, we found that systematic overdispersion of the variability over the Poisson limit was present at smaller cell sizes when the system was stimulated by tunicamycin but not estradiol (Supplementary Fig. 14). These data point to an increase in global cellular variability under stressful conditions.

DISCUSSION

We developed technology to measure the quantitative temporal profiles of molecular phenotypes and growth dynamics in

stimulus-response experiments simultaneously. By combining several subpopulations in the same well, either by mixing strains with different genetic backgrounds or when subpopulations arose as a consequence of cell-to-cell variability, we were able to dissect phenotypes such as relative protein stability and growth rates. We also leveraged the high-throughput nature of our measurements to establish entire time-dependent outputs for a system as a function of dual perturbations. A notable advantage of our technology is that it documents phenotypic variables in single cells and hence provides their distribution across a population. Future exploitation of these dynamically evolving multivariate distributions will help uncover the quantitative features of underlying regulatory processes^{57,58}, including the cell-cycle dependencies of gene expression and protein degradation^{59–62}. We expect that this technology will be instrumental for *in vivo* and dynamic studies of protein turnover, multispecies ecology and dynamic mapping of genetic interactions.

METHODS

Methods and any associated references are available in the [online version of the paper](#).

Note: Any Supplementary Information and Source Data files are available in the online version of the paper.

ACKNOWLEDGMENTS

We thank J. DeRisi for useful conversations, engineering advice and access to equipment; J. Stewart-Ornstein (University of California, San Francisco (UCSF)) for the use of the estradiol-inducible system; and D. Pincus (UCSF) and the Walter lab for the *HAC1*¹ construct. V. Chubukov and C.-S. Chin provided early insight on reactor design and flow cytometry interfacing. This work was funded by the US National Institute of General Medical Sciences (NIGMS) system biology center (P50 GM081879), the David and Lucille Packard Foundation (H.E.-S. and H.L.) and US National Institutes of Health grants R01-GM070808 (H.L.).

AUTHOR CONTRIBUTIONS

I.A.Z., H.E.-S. and H.L. conceived of the hardware setup. I.A.Z. designed, implemented and characterized the hardware setup, control software and mathematical framework. I.A.Z. and A.A.-D. designed and carried over the experiments. I.A.Z., A.A.-D., H.L. and H.E.-S. analyzed and interpreted the data. A.A.-D. cloned the strains necessary for the experiments. I.A.Z., A.A.-D., H.L. and H.E.-S. prepared the manuscript.

COMPETING FINANCIAL INTERESTS

The authors declare no competing financial interests.

Reprints and permissions information is available online at <http://www.nature.com/reprints/index.html>.

- Zhang, Q. & Andersen, M.E. Dose response relationship in anti-stress gene regulatory networks. *PLoS Comput. Biol.* **3**, e24 (2007).
- Muzzey, D. & van Oudenaarden, A. Quantitative time-lapse fluorescence microscopy in single cells. *Annu. Rev. Cell Dev. Biol.* **25**, 301–327 (2009).
- Calvert, M.E.K., Lannigan, J.A. & Pemberton, L.F. Optimization of yeast cell cycle analysis and morphological characterization by multispectral imaging flow cytometry. *Cytometry A* **73**, 825–833 (2008).
- DeRisi, J.L., Iyer, V.R. & Brown, P.O. Exploring the metabolic and genetic control of gene expression on a genomic scale. *Science* **278**, 680–686 (1997).
- Nagalakshmi, U. *et al.* The transcriptional landscape of the yeast genome defined by RNA sequencing. *Science* **320**, 1344–1349 (2008).
- Pierce, S.E. *et al.* A unique and universal molecular barcode array. *Nat. Methods* **3**, 601–603 (2006).
- Cookson, S., Ostroff, N., Pang, W.L., Volfson, D. & Hasty, J. Monitoring dynamics of single-cell gene expression over multiple cell cycles. *Mol. Syst. Biol.* **1**, 2005.0024 (2005).
- Jacquet, M., Renault, G., Lallet, S., De Mey, J. & Goldbeter, A. Oscillatory nucleocytoplasmic shuttling of the general stress response transcriptional activators Msn2 and Msn4 in *Saccharomyces cerevisiae*. *J. Cell Biol.* **161**, 497–505 (2003).

9. Newman, J.R.S. *et al.* Single-cell proteomic analysis of *S. cerevisiae* reveals the architecture of biological noise. *Nature* **441**, 840–846 (2006).
10. Blomberg, A. Measuring growth rate in high-throughput growth phenotyping. *Curr. Opin. Biotechnol.* **22**, 94–102 (2011).
11. Zaslaver, A. *et al.* A comprehensive library of fluorescent transcriptional reporters for *Escherichia coli*. *Nat. Methods* **3**, 623–628 (2006).
12. McKenna, B.K., Evans, J.G., Cheung, M.C. & Ehrlich, D.J. A parallel microfluidic flow cytometer for high-content screening. *Nat. Methods* **8**, 401–403 (2011).
13. Chin, C.-S., Chubukov, V., Jolly, E.R., DeRisi, J. & Li, H. Dynamics and design principles of a basic regulatory architecture controlling metabolic pathways. *PLoS Biol.* **6**, e146 (2008).
14. Levy, S. *et al.* Strategy of transcription regulation in the budding yeast. *PLoS ONE* **2**, e250 (2007).
15. Schimke, R.T. & Doyle, D. Control of enzyme levels in animal tissues. *Annu. Rev. Biochem.* **39**, 929–976 (1970).
16. Belle, A., Tanay, A., Bitincka, L., Shamir, R. & O'Shea, E.K. Quantification of protein half-lives in the budding yeast proteome. *Proc. Natl. Acad. Sci. USA* **103**, 13004–13009 (2006).
17. Leveau, J.H. & Lindow, S.E. Predictive and interpretive simulation of green fluorescent protein expression in reporter bacteria. *J. Bacteriol.* **183**, 6752–6762 (2001).
18. Subramanian, S. & Srien, F. Quantitative analysis of transient gene expression in mammalian cells using the green fluorescent protein. *J. Biotechnol.* **49**, 137–151 (1996).
19. Warner, J.B. & Lolkema, J.S. LacZ-promoter fusions: the effect of growth. *Microbiology* **148**, 1241–1243 (2002).
20. Kawahara, T., Yanagi, H., Yura, T. & Mori, K. Endoplasmic reticulum stress-induced mRNA splicing permits synthesis of transcription factor Hac1p/Ern4p that activates the unfolded protein response. *Mol. Biol. Cell* **8**, 1845–1862 (1997).
21. Buchberger, A., Bukau, B. & Sommer, T. Protein quality control in the cytosol and the endoplasmic reticulum: brothers in arms. *Mol. Cell* **40**, 238–252 (2010).
22. Haynes, C.M., Titus, E.A. & Cooper, A.A. Degradation of misfolded proteins prevents ER-derived oxidative stress and cell death. *Mol. Cell* **15**, 767–776 (2004).
23. Travers, K.J. *et al.* Functional and genomic analyses reveal an essential coordination between the unfolded protein response and ER-associated degradation. *Cell* **101**, 249–258 (2000).
24. Steffen, K.K. *et al.* Ribosome deficiency protects against ER stress in *Saccharomyces cerevisiae*. *Genetics* **191**, 107–118 (2012).
25. Delic, M. *et al.* Oxidative protein folding and unfolded protein response elicit differing redox regulation in endoplasmic reticulum and cytosol of yeast. *Free Radic. Biol. Med.* **52**, 2000–2012 (2012).
26. Pollard, M.G., Travers, K.J. & Weissman, J.S. Ero1p: a novel and ubiquitous protein with an essential role in oxidative protein folding in the endoplasmic reticulum. *Mol. Cell* **1**, 171–182 (1998).
27. Latimer, P. Light scattering vs. microscopy for measuring average cell size and shape. *Biophys. J.* **27**, 117–126 (1979).
28. Tzur, A., Moore, J.K., Jorgensen, P., Shapiro, H.M. & Kirschner, M.W. Optimizing optical flow cytometry for cell volume-based sorting and analysis. *PLoS ONE* **6**, e16053 (2011).
29. Mullaney, P.F. & Dean, P.N. The small angle light scattering of biological cells. *Biophys. J.* **10**, 764–772 (1970).
30. Münch, T., Sonnleitner, B. & Fiechter, A. The decisive role of the *Saccharomyces cerevisiae* cell cycle behaviour for dynamic growth characterization. *J. Biotechnol.* **22**, 329–351 (1992).
31. Delgado, M.L. *et al.* The glyceraldehyde-3-phosphate dehydrogenase polypeptides encoded by the *Saccharomyces cerevisiae* *TDH1*, *TDH2* and *TDH3* genes are also cell wall proteins. *Microbiology* **147**, 411–417 (2001).
32. Pratt, J.M. *et al.* Dynamics of protein turnover, a missing dimension in proteomics. *Mol. Cell. Proteomics* **1**, 579–591 (2002).
33. Bachmair, A. & Varshavsky, A. The degradation signal in a short-lived protein. *Cell* **56**, 1019–1032 (1989).
34. Varshavsky, A. The early history of the ubiquitin field. *Protein Sci.* **15**, 647–654 (2006).
35. Lopez, A.D. *et al.* Proteasomal degradation of Sfp1 contributes to the repression of ribosome biogenesis during starvation and is mediated by the proteasome activator Blm10. *Mol. Biol. Cell* **22**, 528–540 (2011).
36. Varshavsky, A. Ubiquitin fusion technique and related methods. *Methods Enzymol.* **399**, 777–799 (2005).
37. Bachmair, A., Finley, D. & Varshavsky, A. *In vivo* half-life of a protein is a function of its amino-terminal residue. *Science* **234**, 179–186 (1986).
38. Tobias, J.W. & Varshavsky, A. Cloning and functional analysis of the ubiquitin-specific protease gene *UBP1* of *Saccharomyces cerevisiae*. *J. Biol. Chem.* **266**, 12021–12028 (1991).
39. Baker, R.T., Tobias, J.W. & Varshavsky, A. Ubiquitin-specific proteases of *Saccharomyces cerevisiae*. *J. Biol. Chem.* **267**, 23364–23375 (1992).
40. Shcherbo, D. *et al.* Far-red fluorescent tags for protein imaging in living tissues. *Biochem. J.* **418**, 567–574 (2009).
41. Vembar, S.S. & Brodsky, J.L. One step at a time: endoplasmic reticulum-associated degradation. *Nat. Rev. Mol. Cell Biol.* **9**, 944–957 (2008).
42. Chen, M., Gutierrez, G.J. & Ronai, Z.A. Ubiquitin-recognition protein Ufd1 couples the endoplasmic reticulum (ER) stress response to cell cycle control. *Proc. Natl. Acad. Sci. USA* **108**, 9119–9124 (2011).
43. Hanna, J., Meides, A., Zhang, D.P. & Finley, D. A ubiquitin stress response induces altered proteasome composition. *Cell* **129**, 747–759 (2007).
44. Onodera, J. & Ohsumi, Y. Autophagy is required for maintenance of amino acid levels and protein synthesis under nitrogen starvation. *J. Biol. Chem.* **280**, 31582–31586 (2005).
45. Carvalho, P., Stanley, A.M. & Rapoport, T.A. Retrotranslocation of a misfolded luminal ER protein by the ubiquitin-ligase Hrd1p. *Cell* **143**, 579–591 (2010).
46. Yewdell, J.W., Lacsina, J.R., Rechsteiner, M.C. & Nicchitta, C.V. Out with the old, in with the new? Comparing methods for measuring protein degradation. *Cell Biol. Int.* **35**, 457–462 (2011).
47. Eden, E. *et al.* Proteome half-life dynamics in living human cells. *Science* **331**, 764–768 (2011).
48. Lévy, F., Johnsson, N., Rüménapf, T. & Varshavsky, A. Using ubiquitin to follow the metabolic fate of a protein. *Proc. Natl. Acad. Sci. USA* **93**, 4907–4912 (1996).
49. Anderson, J.C., Voigt, C.A. & Arkin, A.P. Environmental signal integration by a modular AND gate. *Mol. Syst. Biol.* **3**, 133 (2007).
50. Müller, D. & Stelling, J. Precise regulation of gene expression dynamics favors complex promoter architectures. *PLoS Comput. Biol.* **5**, e1000279 (2009).
51. Aldridge, B.B., Gaudet, S., Lauffenburger, D.A. & Sorger, P.K. Lyapunov exponents and phase diagrams reveal multi-factorial control over TRAIL-induced apoptosis. *Mol. Syst. Biol.* **7**, 553 (2011).
52. Birtwistle, M.R. *et al.* Emergence of bimodal cell population responses from the interplay between analog single-cell signaling and protein expression noise. *BMC Syst. Biol.* **6**, 109 (2012).
53. Bollenbach, T. & Kishony, R. Resolution of gene regulatory conflicts caused by combinations of antibiotics. *Mol. Cell* **42**, 413–425 (2011).
54. Wang, Y., O'Malley, B.W. & Tsai, S.Y. A regulatory system for use in gene transfer. *Proc. Natl. Acad. Sci. USA* **91**, 8180–8184 (1994).
55. Stewart-Ornstein, J., Weissman, J.S. & El-Samad, H. Cellular noise regulons underlie fluctuations in *Saccharomyces cerevisiae*. *Mol. Cell* **45**, 483–493 (2012).
56. McIsaac, R.S. *et al.* Fast-acting and nearly gratuitous induction of gene expression and protein depletion in *Saccharomyces cerevisiae*. *Mol. Biol. Cell* **22**, 4447–4459 (2011).
57. Neuert, G. *et al.* Systematic identification of signal-activated stochastic gene regulation. *Science* **339**, 584–587 (2013).
58. Munsky, B., Trinh, B. & Khammash, M. Listening to the noise: random fluctuations reveal gene network parameters. *Mol. Syst. Biol.* **5**, 318 (2009).
59. Howlett, N.G. & Avery, S.V. Flow cytometric investigation of heterogeneous copper-sensitivity in asynchronously grown *Saccharomyces cerevisiae*. *FEMS Microbiol. Lett.* **176**, 379–386 (1999).
60. Kafri, R. *et al.* Dynamics extracted from fixed cells reveal feedback linking cell growth to cell cycle. *Nature* **494**, 480–483 (2013).
61. Knijnenburg, T.A. *et al.* A regression model approach to enable cell morphology correction in high-throughput flow cytometry. *Mol. Syst. Biol.* **7**, 531 (2011).
62. Brown, M.R. *et al.* Flow-based cytometric analysis of cell cycle via simulated cell populations. *PLoS Comput. Biol.* **6**, e1000741 (2010).

ONLINE METHODS

Automated flow cytometry hardware setup. The automated flow cytometry hardware setup consists of a three-laser flow cytometer (LSR II, Becton Dickinson (BD)), a liquid handler (Multimek 96, Beckman Coulter) and an open deep-well plate magnetic heater/shaker (Variomag Teleshake, Inheco). Plates are transferred between these three devices with a robotic arm (Plate Crane XL, Hudson Robotics). All hardware is secured on a steel breadboard and partially enclosed with an aluminum frame to decrease temperature fluctuations and reduce contamination. Cell cultures are grown in a 1-mL 96-well polystyrene plate (Riplate, Ritter) that is agitated at 900 r.p.m. and kept at 30 °C in the heater/shaker.

In our setup, the liquid handler takes a 10- to 100- μ L sample (sample volume, V_s) of the 400- to 600- μ L cell culture (culture volume, V_c) every 10–20 min (sampling frequency, t_s). A volume of fresh medium equal to the sample volume is added at every time point to maintain a constant culture volume. The sample is then placed in a second shallow 96-well microplate (Model 3795, Corning) containing 70 μ L of Tris-EDTA buffer (pH = 7.4). The diluted samples are then measured using a high-throughput sampler (BD High Throughput Sampler 338301, BD) to inject samples into the flow cytometer. The parameters t_s , V_s and V_c determine an effective culture dilution rate (d_2) that can be arbitrarily and dynamically set for each experiment so as to achieve the desired concentration of cells and to accommodate different growth rates (Supplementary Fig. 1). The values used in our experiments are $V_c = 500 \mu\text{L}$, $V_s = 30 \mu\text{L}$ and $t_s = 20 \text{ min}$, resulting in $d_2 = 0.94$. This equals a mean residence time of a volume element in the culture ($t_{1/2}$) of approximately 4 h, which means that the observed number of cells of a strain growing with a doubling time of 4 h will remain constant, whereas strains that are faster or slower either accumulate or are washed away.

The stimulus event, which takes place at t_0 , consists of the medium plate being instantaneously swapped for a medium plate containing the stimulus at a titer that brings the effective concentration of stressor to $1\times$ in the culture. This titer equals the dilution factor of the medium (d_1) multiplied by the desired concentration of stressor (d_1X). This is followed for later dilution events with a medium plate with $1\times$ titer for the response phase. A typical experiment consists of an outgrowth phase of 3 h followed by response phase lasting 8 h.

Pipette tips are reused through the experiment and washed with 50% ethanol and water between samples.

Reproducibility experiments showed no cell carryover between wells, and measurements of cell division rate and fluorescence were reproducible to better than a few percent with no internal controls (Supplementary Fig. 1b–d). Although we have not used internal controls in the data presented here, this and other experimental designs decrease error substantially. Because the figures presented are dependent on the particular experimental design and data analysis strategy, we report reproducibility data on only the most basic measurements. Although there was no appreciable bias or unevenness in the heating of individual wells as measured using a thermocouple sensor, there was a reproducible vertical temperature gradient of about 1 °C in each well (data not shown).

Software and data processing. We use a custom-written software for data acquisition and control of each piece of hardware

independently and for their coordination (LabVIEW, National Instruments). A personal computer runs concurrent threads that control the flow cytometer, its high-throughput sampler, the liquid handler, the robotic arm and the heater/shaker where cells grow. Sensors embedded in each piece of hardware report on their individual state and allow for a master thread to coordinate the sampling, dilution and measurement of cell density and fluorescence using the flow cytometer. An Ethernet connection to the flow cytometer, set up to run continuously, provides access of the stream of data events that make up the raw flow cytometry data set. The continuous data stream is displayed in real time as it is acquired and simultaneously stored as individual binary data files for offline analysis. Offline data analysis is performed using custom scripts that generate histograms for all various parameters and computes summary statistics such as fluorescence distributions and equivalent cell densities (Matlab R2012b, MathWorks). These data are first processed to remove outliers by removing events with no fluorescence, events with forward-scatter (FSC) values of less than 5,000 and events outside of 4 s.d. of the joint side scatter (SSC) and FSC. Fluorescence is corrected by cell size using the SSC values for each event⁵⁵. Using cell sorting and automated microscopy, we found that the SSC parameter is a good surrogate of cell volume (Supplementary Fig. 2) and is thus a good surrogate for cell size. Cell densities are estimated from the (Poisson) rate at which cells enter the flow cytometer. We do this by fitting an exponential distribution to interarrival times (τ_i) for each well to determine the mean $\langle\tau\rangle$. Cell density N is then calculated as $(\langle\tau\rangle \times L)^{-1}$, where L is the sample injection flow rate (usually 1 $\mu\text{L/s}$).

Plasmids and strains. All plasmids and oligonucleotides used in this study are listed in Supplementary Tables 2 and 3. The Ub-Tyr-GFP³⁶ construct is driven by a crippled *CYC1* promoter containing four *cis*-acting UPRE motifs. The 4XUPRE synthetic promoter contains four copies of the UPRE motif CAGCGTG⁶³, which is a known binding target for the transcription factor Hac1p. All plasmids used in this work are single-genomic integration plasmids.

The promoter of *CYC1* was amplified from *S. cerevisiae* (strain W303a) genomic DNA with Elongase Enzyme Mix (Life Technologies) and cloned between PspOMI and XhoI sites in a pNH605 plasmid. GFP was then cloned between XhoI and BamHI sites. The region containing the UPRE elements was amplified with Elongase Enzyme Mix from the Ub-Tyr-GFP plasmid and was cloned into KpnI and PspOMI restriction sites, resulting in plasmid pAAD53. Stress reporters were constructed by amplifying the promoters of *SSA1*, *HSP12*, *HSP82*, *HOR2*, *GPD1* and *ERO1* from genomic DNA and cloned between PspOMI and XhoI sites in a plasmid containing the GFP ORF, resulting in plasmids pAAD7–pAAD12. The splicing reporter is a modified *HAC1* construct in which the first exon has been replaced by GFP⁶⁴. The barcoding construct was assembled by cloning the promoter of *TDH3* between PspOMI and XhoI restriction sites followed by mKate2 between XhoI and BamHI sites into a plasmid containing the *HIS3* coding sequence from *Candida albicans*. This plasmid was amplified with primers containing homology regions to the *CAN1* locus and then transformed into yeast to get the barcoded strain. The rest of the plasmids we sequentially transformed into the W303a strain by linearizing them and making the yeast cells

competent with a standard lithium acetate method. All the resulting strains are listed in **Supplementary Table 1**.

Growth conditions. Starting from single colonies picked from YPD (yeast extract, peptone, 2% (w/v) glucose) agar plates, yeast cultures were inoculated and grown for 24 h in exponential phase at 30 °C in YPD liquid medium. Before the multiplexed experiment, the two strains were combined at an approximate ratio of 1:1 and diluted to a total of a density of 10⁶ cells/mL. 500 µL of the mix was transferred into a 96-deep-well polycarbonate plate.

Before the start of the experiment, cells were continuously grown while being diluted with fresh YPD medium that did not contain any stimulus. Stimuli were applied by subjecting to combinations of an exogenous inducer (β-estradiol, Sigma-Aldrich) and an ER stressor (tunicamycin, Calbiochem). Serial dilutions of a 33.3× solution of either estradiol or tunicamycin were combined in equal amounts into a 96-well 2-mL block, resulting in a 16.6× set of solutions. These solutions replaced the fresh medium in the liquid handler in the stimulus event. A further 1:16.6 dilution was made to obtain the 1× solution that was used to keep the titer constant during the response phase.

To confirm that cells do not undergo stress by exposure to the liquid handling shear forces associated with constant dilution, we measured the fluorescence of several stress-responsive transcriptional reporters that reflect the activity of various stress-responsive transcription factors for ER stress (*HAC1* splicing rate⁶⁴, pERO1 and p4XUPRE transcription), general stress (pHSP12), heat shock (pSSA1 and pHSP82) and high osmolality (pGPD1, pHOR2). **Supplementary Figure 15** shows time-course data with no treatment (control), UPR activation (80 nM estradiol) and ER stress (5 µg/mL tunicamycin). These data demonstrate that liquid handling and the various manipulations in our setup did not elicit stress responses, as sensed by these various pathways.

Inducible heterologous gene expression system. The inducible system consists of a chimeric transcription factor construct (plasmid pPW2078) and a gene expression construct (pPW2085), both of which are integrated into the genome sequentially and at different loci.

The chimeric transcription factor (GERM construct) is a fusion of the Gal4p DNA-binding domain (GAL4[DBD]), the human estradiol receptor lipid-binding domain (ER[LBD]) and the Msn2 activation domain (MSN2[AD]) (GERM). The expression

of the GERM construct is driven by the *ADHI* promoter⁵⁵. The gene expression system consists of the intronless allele of *HAC1* (*HAC1ⁱ*, an active mRNA form of *HAC1* not subject to Ire1 regulation^{65,66}) coding sequence driven by the *GAL1* promoter. Upon estradiol addition, the GERM transcription factor localizes into the nucleus and activates the transcription of genes driven by *GAL4P* binding site-containing promoters, including the *HAC1ⁱ* construct.

Cell size measurements. FSC and SSC were measured and used as a proxy for cell volume (**Supplementary Fig. 2a**). To establish the correspondence between flow cytometry parameters and cellular parameters, we sorted and, using 3% formaldehyde, fixed an exponentially growing cell population. Cells were sorted on the basis of their forward-scatter (FSC-A) value, and their volume was estimated using bright-field microscopy with a 40× objective. Cells were automatically located in the image, and their volume was estimated by revolving their contour along their longest axis of symmetry. The plot in **Supplementary Figure 2b** shows the estimated robust mean of the cell volume as a function of the centroid of the FSC-A gate (blue trace). For reference purposes, the population histogram is shown (green).

Cell viability assay. Five 50-µL TE-diluted samples from our setup were plated into YPD agar plates. These samples corresponded to the cells exposed to the individual stimuli and combinations of them, as well as a control. Plates were left in an incubator at 30 °C, and after 2 d, images were taken. Colony-forming units were counted from the images with an automated image analysis by taking an equivalent squared area from each of the pictures (**Supplementary Fig. 3**).

63. Mori, K., Ogawa, N., Kawahara, T., Yanagi, H. & Yura, T. Palindrome with spacer of one nucleotide is characteristic of the *cis*-acting unfolded protein response element in *Saccharomyces cerevisiae*. *J. Biol. Chem.* **273**, 9912–9920 (1998).
64. Pincus, D. *et al.* BiP binding to the ER-stress sensor Ire1 tunes the homeostatic behavior of the unfolded protein response. *PLoS Biol.* **8**, e1000415 (2010).
65. Cox, J.S. & Walter, P. A novel mechanism for regulating activity of a transcription factor that controls the unfolded protein response. *Cell* **87**, 391–404 (1996).
66. Sidrauski, C. & Walter, P. The transmembrane kinase Ire1p is a site-specific endonuclease that initiates mRNA splicing in the unfolded protein response. *Cell* **90**, 1031–1039 (1997).